Journal of Computers Vol. 28, No. 5, 2017, pp. 327-337
doi:10.3966/199115992017102805028

Analysis of MIMO SAR Imaging Algorithm Based on Complete Complementary Sequence and Phase Compensation

Shu-Feng Li[1*], Hong-Da Wu[1] and Li-Biao Jin[1]

[1] School of Information Engineering, Communication University of China,
Beijing 100024, CHN
{lishufeng, libiao}@cuc.edu.cn
cucwhd@163.com

Received 24 July 2017; Revised 24 August 2017; Accepted 24 September 2017

Abstract. The CC-S (Complete Complementary Sequence) is composed of several complementary orthogonal sequences, which is satisfied with the requirement of the orthogonal Multiple-Input Multiple-Output (MIMO) radar signals. Aimed at the difficulty of high sidelobe in Synthetic Aperture Radar (SAR) imaging processing, an approach of depressing sidelobe output based on CC-S in MIMO SAR system was proposed. The model for orthogonal MIMO radar transmitting signals and the corresponding match filter were established in this paper. Equivalent phase compensation theory is used to carry out compensation for signal phase shift. The MIMO SAR imaging algorithm with CC-S was deduced. The simulation results demonstrate that the imaging performance of CC-S employed in orthogonal MIMO radar system is much better than that with traditional Linear Frequency Modulation (Chirp) signal and Barker signal, by which the feasibility and validity of CC-S applied in orthogonal MIMO SAR system are justified.

Keywords: complete complementary sequence, MIMO, SAR

1 Introduction

The Multiple-Input Multiple-Output (MIMO) radar improves the performance by multiple transmitting antennas transmitting signals to the target, multiple receiving antennas receiving signals from the target and carrying out the data process of signals received. Based on the current research on the MIMO radar, transmitting antennas of the orthogonal MIMO radar transmit the orthogonal waveform sets; the receiving ends recover transmitted signal components by matched filtering, in which the design of transmitted signals directly influences the orthogonal MIMO radar system performance. Time synchronization of the transceiver end is also an emphasis [1]. In order to suppress interference and improve multiple targets resolution, a good correlation function between transmitted signals is needed, which meets complete orthogonality; that is, the side-lobe of aperiodic auto-correlation function is zero and the main-lobe and side-lobe of aperiodic cross-correlation function is both zero. Currently the orthogonal MIMO radar mainly uses the poly-phase coding [2] and orthogonal frequency coding [3-4], which still cannot meet complete orthogonality between transmitted signals despite that the correlation functions of these two coding possess the rather low side-lobe performance. Theoretical researches showed that the sequence which meets complete orthogonality does not exist in the traditional single-code domain. Therefore the appearance of Complete Complementary Sequence (CCS) opened up a new direction for choosing the orthogonality MIMO radar signal.

Synthetic Aperture Radar (SAR) plays an important role in radar imagining due to all-weather, all-time and long-distance working [5-6]. Recently, with the MIMO radar development, applying it to target imaging is becoming an emphasis of MIMO radar [7-8]. Duan, Wang and Ma [7] dealt with movement compensation in ISAR imaging by deterministic relation between multiple MIMO radar matrix elements. Wang, Su and Zhu [8] mainly analyzed the relationship between MIMO radar transceiver array

* Corresponding Author

configuration, imaging performance and spatial spectral domain filling. These references both focused on the air target imaging performance of ground MIMO radar. This paper mainly discussed the ground target imaging of airborne MIMO SAR. Since the MIMO SAR system requires that transmitted signals satisfy orthogonality, exploring orthogonal signals that apply well for MIMO SAR becomes a key concentration in practical application.

This paper primarily analyzed a CCS-based MIMO SAR imaging method, utilizing the property of CCS correlation function that it has no side-lobes, which meant the high peak side-lobe rate could be easily achieved after range compression without suppressing the side-lobe. For the traditional SAR system based on Chirp signal, the peak side-lobe rate is normally raised by window function, yet resulting in main-lobe expansion and resolution reduction. The CCS-based MIMO ASR, however, due to the deprivation of window function, promises the high peak side-lobe rate and good resolution simultaneously, improving the SAR system performance.

2 MIMO SAR Imaging Analysis

2.1 CCS Signal Model

The CCS transmitting sequence: complementary pairs are transmitted in two pulse repetition periods, which is shown in Fig. 1.

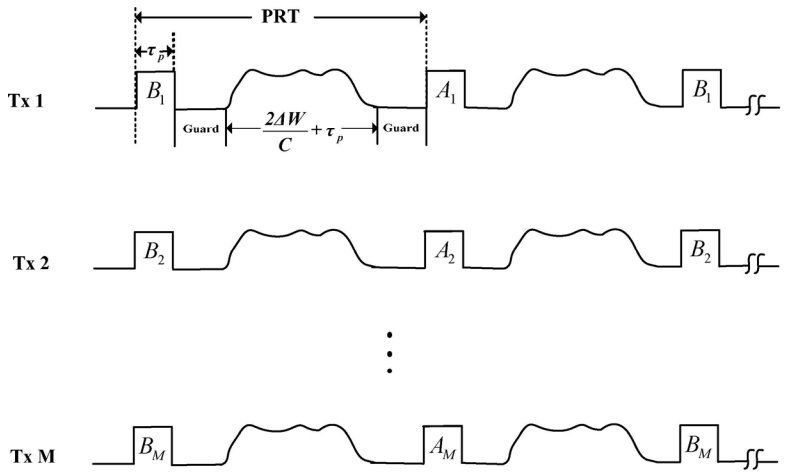

Fig. 1. CCS time sequence model

From Fig. 1, since the minimum time of receiving echo signal is $2\Delta W / C + \tau_p$, where ΔW is the ground length of radar irradiation and C is the wave speed, if the length of protection band is $3\tau_p$, the maximum value of pulse repetition frequency is:

$$PRF_{\max} = \left(\frac{2\Delta W}{C} + 5\tau_p \right)^{-1} \tag{1}$$

Where A_m and B_m $(0 \le m \le M-1)$ are a pair of complementary sequences and T represents the delay time. The M complementary sequences $\{A_m, B_m\}$ with the length of L is defined as below:

$$\begin{cases} A_m = (a_m^0, a_m^1, \cdots, a_m^{L-1}) \\ B_m = (b_m^0, b_m^1, \cdots, b_m^{L-1}) \end{cases} \tag{2}$$

Where $\{(A_0, B_0), (A_1, B_1), \cdots, (A_{M-1}, B_{M-1})\}$ meets the complete orthogonality as below:

$$R_{A_mA_m}(l) + R_{B_mB_m}(l) = \begin{cases} 2L & \tau = 0 \\ 0 & \tau \neq 0 \end{cases} \tag{3}$$

$$R_{A_nA_n}(l) + R_{B_nB_n}(l) = \begin{cases} 2L & \tau = 0 \\ 0 & \tau \neq 0 \end{cases} \tag{4}$$

When $0 \le m \ne n < M$,

$$R_{A_mA_n}(l) + R_{B_mB_n}(l) = 0 \qquad \forall \tau \tag{5}$$

$\{A_m, B_m\}$ and $\{A_n, B_n\}$ make a pair of CCS, where $R_{A_mA_m}(\tau)$ is the auto-correlation function of sequence A_m, $R_{A_mA_n}(\tau)$ is the cross-correlation function between A_m and A_n. Eq(3) and Eq(4) represent the auto-correlation function of CCS, Eq(5) represents the cross-correlation function of CCS and l represents the discreet time offset. Therefore A_m and B_m make CCS sets.

From Fig. 1, signal A_m, B_m are transmitted alternatively in the m antenna, which means the transmitted signal $s_m(\tau)$ of the m transmitting antenna is shown as below:

$$\begin{aligned} s_m(\tau) &= \sum_{l=0}^{L-1} [a_m^l \cdot rect(\frac{\tau - l \cdot T_c}{\tau_p}) + b_m^l \cdot rect(\frac{\tau - T - l \cdot T_c}{\tau_p})] \cdot e^{j2\pi f_c \tau} \\ &= [s_{A_m}(\tau) + s_{B_m}(\tau - T)] \cdot e^{j2\pi f_c \tau} \end{aligned} \tag{6}$$

Where T is the pulse repetition period, T_c represents the sub-pulse width, $\tau_p = L \cdot T_c$ is the transmitted pulse width, f_c is the carrier wave frequency and $rect(t)$ is the rectangular window function, whose value is 1 when $0 \le t \le \tau_p$ and otherwise 0.

By utilizing CCS, the complete orthogonality is satisfied, making it possible for range-dimensional and azimuth-dimensional imaging to work independently. The imaging process refers to Chen and Zhang [9].

2.2 Equivalent Phase Center Compensation

In order to deal with the problem that the azimuth resolution and swath width cannot be raised simultaneously in MIMO SAR imaging mode, Currie [10] proposed a method that one transmitter is used in the transmitting end, and multiple receivers in the receiving end to realize Multiple Azimuth Beam (MAB). Its principle was to decrease time dimension samples by increasing azimuth spatial dimension samples, promising the azimuth resolution and improving the swath width simultaneously. Suess, Grafmueller and Zahn [11] came up with an azimuth single-transmitting multiple-receiving SAR mode, which meant multiple sub-apertures were used to transmit in the azimuth position and only single sub-aperture was used to transmit and multiple sub-apertures to receive echo signals. Subsequently MIMO SAR appeared [12], which resulted in spatial sampling rate increase, swath width expansion and azimuth resolution improvement. Unfortunately, the azimuth non-uniform sampling in this method caused Doppler ambiguity. In order to solve this problem, some relatively mature ambiguity resolution methods have been proposed and the following section analyzed uniform sampling.

MIMO SAR possesses the same principle with the regular single-transmitting multiple-receiving system. Along the azimuth the radar antenna consists of multiple sub-antennas; every sub-antenna has the same size and beam width and the radiation targets are from the same areas. The principle is shown in Fig. 2.

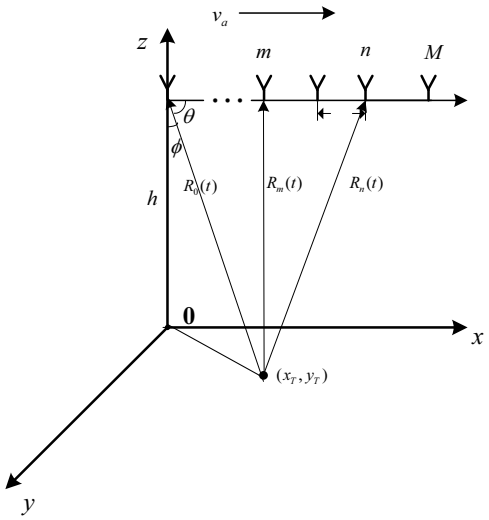

Fig. 2. Antenna array model

Where M is the total number of antennas, d is the distance between near antennas, $R(t)$ is the slant range of antenna 1 at the time t, $R(t+(m-1)d/v_a)$ and $R(t+(n-1)d/v_a)$ are the slant ranges of antenna m and n at the time t respectively, $R(t+(m+n-2)d/2/v_a)$ is the equivalent slant range of antenna m and n, θ is the angle between reference slant range $R(t)$ and the antenna normal direction, and v_a is the speed.

Every transmitting antenna transmits different signals. After signals are reflected by the target, every receiver could receive echo signals transmitted by all transmitters, split different echo signals and arrange them along the azimuth direction, largely improving the spatial sampling rate. Besides, since the equivalent phase center is applied when time sampling is replaced by spatial sampling, the phase center error is introduced. Therefore the equivalent phase center error is in need of compensation, where the system could be equivalent to single-transmitting single-receiving mode, ranging data in a slow-time sequence according to array configuration [13] In this case, the MIMO SAR system of M sub-apertures will produce M^2 sampling points in a Pulse Repetition Period (PRT), where the sampling point is considered as one when the azimuth positions coincide. The system can generate different efficient sampling points according to the different antenna configuration.

Fig. 3 shows the array configuration when the transmitting matrix element distance is different from the receiving matrix element distance. When the array configuration is $d_t = Nd_r$ or $d_r = Md_t$, where d_t is the transmitting matrix element distance and d_r is the receiving matrix element distance, the configuration can make the equivalent virtual matrix element number reach MN during one transceiver process of MIMO SAR.

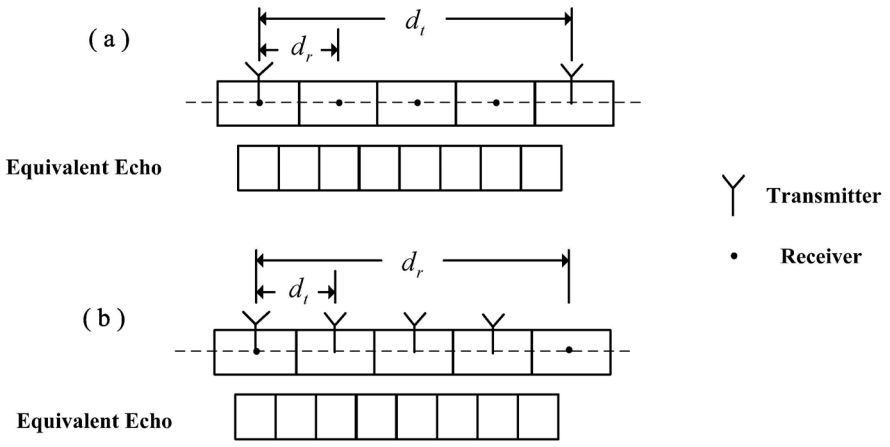

Fig. 3. Transceiver split configuration

The antenna array configuration is shown in Fig. 4. The transmitting and receiving antennas are in the same place when the aperture distance is even 2*M*-1 efficient sampling points are generated, increasing the sampling points to which 2M-1 times the single-transmitting single-receiving system and promising the azimuth resolution and broadening swath simultaneously. Expect for the configuration that the transmitting and receiving antennas are in the same place, different antenna configurations can result in different sampling points.

Fig. 4 demonstrates the equivalent phase center principle taking 4 transceiver antennas as the example.

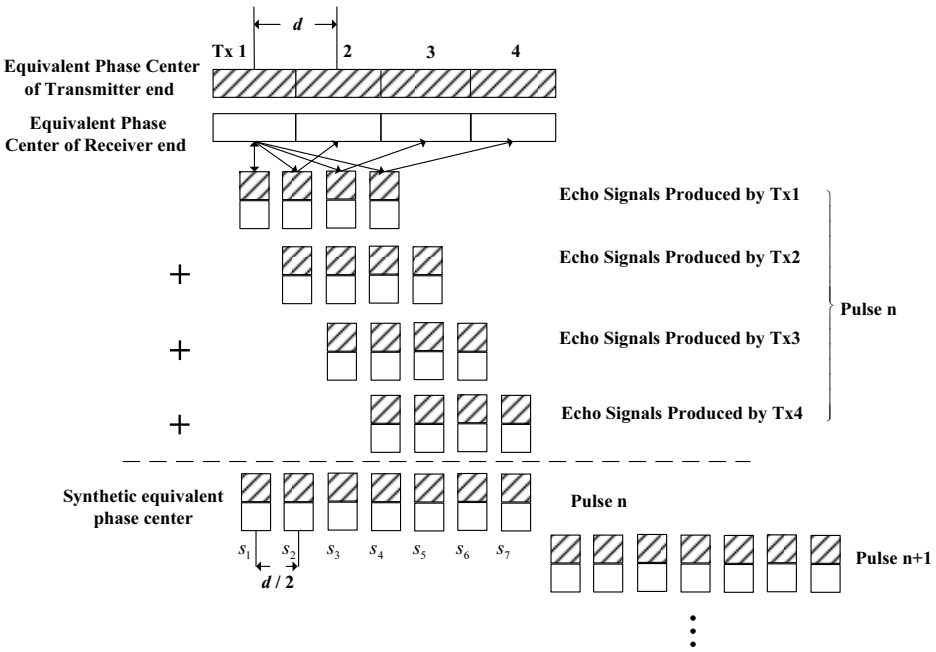

Fig. 4. MIMO SAR equivalent phase center

If the bidirectional transceiver phase center is defined as the middle point of a line from the transmitting phase center to receiving phase center, as Fig. 4 shows, all 4 sub-antennas transmit and receive signals and they make 7 spatial samplings to the target during every PRT. In every PRT, the flying distance satisfies the following equation:

$$v_a \cdot PRT = (2M-1)d/2 \tag{7}$$

That is:

$$PRF = \frac{v_a}{(2M-1)\frac{d}{2}} \tag{8}$$

Although the said equivalent phase center approach keeps its position unchanged, there exists a certain phase difference between two echo signals because the equivalent phase center is from different transmitting and receiving antennas. Currie and Brown [14] showed a deduction method using the single-transmitting multiple-receiving phase difference.

As Fig. 3 shows, taking the first transmitting antenna as the example, the slant range from its phase center to the ground target is $R(t)$, represented as the Taylor polynomial series：

$$R(t) \approx R_0 - v_a \sin\theta(t-t_0) + \frac{v_a^2 \cos^2\theta}{2R_0}(t-t_0)^2 \tag{9}$$

Where R_0 is the slant range of where reference time t_0 is, $R_0 = h/\cos\varphi$, h is the flying height, φ is the elevation angle, T_s is time for synthesizing the aperture.

Taking the slant range of the first antenna as the reference slant range and deducting the phase course of echo signals, the self-transmitting self-receiving phase course is $\phi_1 = 2\pi \cdot 2R(t)/\lambda$, λ is the carrier

wave length. At time t, the distance from the m antenna to the target $R_m(t)$ is:

$$R_m(t) = R(t + \frac{(m-1)d}{v_a}) \tag{10}$$

Meanwhile, the distance $R_n(t)$ from the target to the n antenna is:

$$R_n(t) = R(t + \frac{(n-1)d}{v_a}) \tag{11}$$

Therefore the slant range of the m antenna both transmitting and receiving is:

$$\begin{aligned} R_{mn} &= R_m(t) + R_n(t) \\ &= R(t + \frac{(m-1)d}{v_a}) + R(t + \frac{(n-1)d}{v_a}) \\ &= 2R(t) + \alpha \cdot \frac{(m+n-2)d}{v_a} + 2\beta \cdot \frac{(m+n-2)d}{v_a}(t - t_0) \\ &\quad + \beta \left[\frac{(m-1)^2 d^2}{v_a^2} + \frac{(n-1)^2 d^2}{v_a^2} \right] \end{aligned} \tag{12}$$

And the equivalent slant range between the m antenna and the n antenna is:

$$\begin{aligned} R_{mn}^{eq} &= 2R(t + \frac{(m+n-2)d}{2v_a}) \\ &= 2R(t) + \alpha \cdot \frac{(m+n-2)d}{v_a} \\ &\quad + 2\beta \cdot \frac{(m+n-2)d}{v_a}(t - t_0) + \beta \frac{(m+n-2)^2 d^2}{2v_a^2} \end{aligned} \tag{13}$$

Combining Eq(12) and Eq(13), we can see that they only have a slight difference of the last item. As a result, the equivalent phase center difference is:

$$\Delta\omega_{mn} = \frac{2\pi(R_{mn}^{eq} - R_{mn})}{\lambda} = \beta \frac{2\pi}{\lambda} \frac{(m-n)^2 d^2}{2v_a^2} \tag{14}$$

From the deduction above, we can know that the phase difference between two arbitrary antennas m and n is $\Delta\omega_{mn}$ and $\Delta\omega_{mn} = \Delta\omega_{nm}$. Under the condition of side-looking, θ is the half beam-width angle.

Applying the equivalent phase principle, from Eq(14), we have $\phi_{mn} = \exp(j\Delta\omega_{mn})$ and $\phi_{mn} = \phi_{nm}$. For the MIMO SAR system of M antennas, define $y_{n.m}$ as the equivalent receiving signal and then the signal after phase compensation is $E_{mn} = y_{n,m} \cdot \phi_{mn}$. According to the arrangement from Reference[11], arrange E_{mn} in the following way, where $m, n \in 1, \cdots, M$, and then the echo signal in a PRT can be described as below:

$$\mathbf{P} = \begin{bmatrix} E_{1,1} & E_{1,2} & \cdots & E_{1,M} & 0 & \cdots & 0 \\ 0 & E_{2,1} & E_{2,2} & \cdots & E_{2,M-1} & 0 & \vdots \\ \vdots & \ddots & \ddots & \ddots & \ddots & \ddots & \vdots \\ 0 & 0 & 0 & E_{M,1} & \cdots & E_{M,M-1} & E_{M,M} \end{bmatrix}_{M \times (2M-1)} \tag{15}$$

From the analysis above, first split the echo signals, then arrange them and take the average of data integration after phase error compensation and superposition, which can be equivalent to the echo signal phase course of a single-antenna system. The imaging flow is shown in Fig. 5.

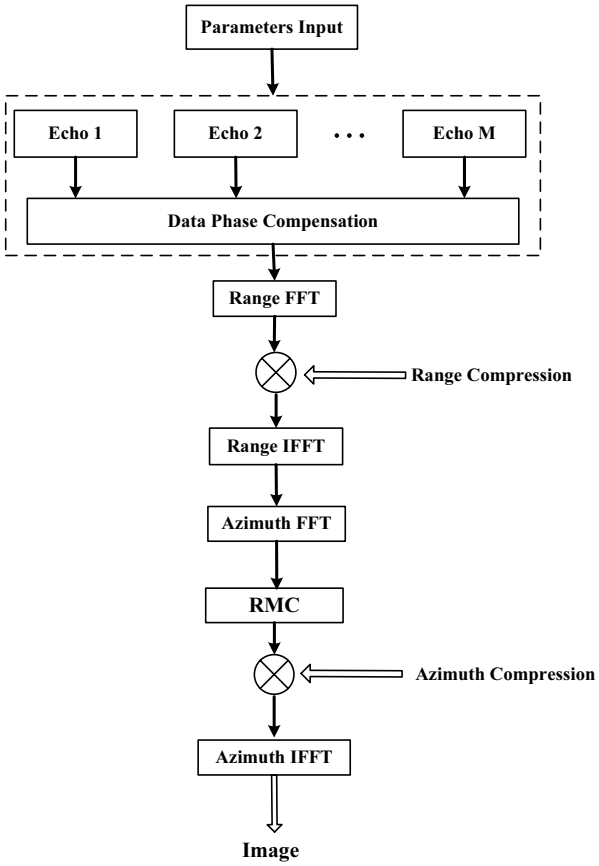

Fig. 5. Imaging flow

3 Simulation Experiment

In order to testify the MIMO SAR imaging technology above, we carried out the following simulation experiment. Taking the double-transmitting double-receiving antenna system as the example, each transmitting matrix element of the radar system transmits the complementary sequence, in which the construction method refers to [15] and the code length is 40. The matrix element configuration is shown as Fig. 2, where the distance d between every antenna is 2m and the elevation angle is 24º. Due to the convenience of analysis, we took the side-looking as the simulation condition. Set the targets 9 ideal point scatters, the scattering amplitude of every scattering point is the same, and other simulation parameters are shown in Table 1.

Table 1. Simulation parameter

simulation parameter	value
wave length	0.018
sub-pulse length (μ s)	0.025
signal band (MHz)	40
signal sampling rate (MHz)	50
Sub-array distance (m)	2
pulse repetition frequency (Hz)	220
flying height (km)	5
speed (m/s)	100

The CCS-based point target imaging result is shown in Fig. 6 (a). From Fig. 6, CCS can be applied to MIMO SAR system and generate the correct image of point target.

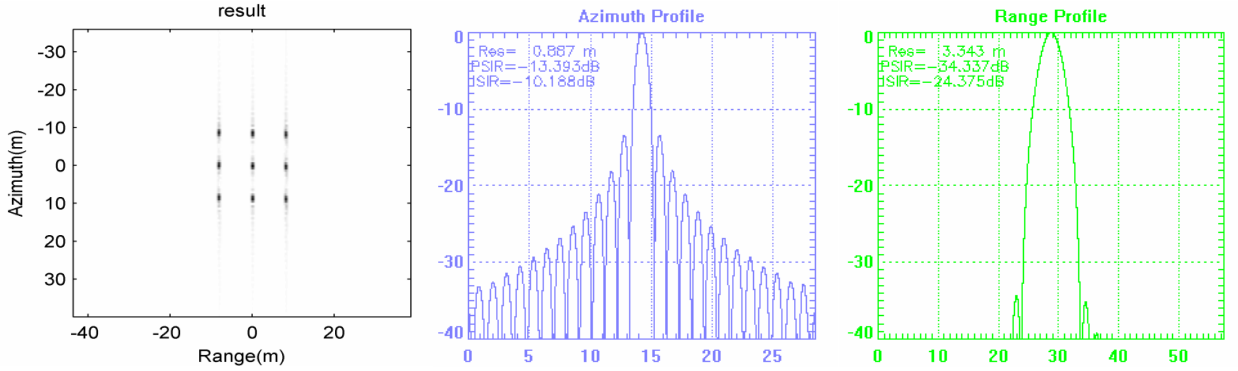

(a) Point target imaging result (b) Azimuth compression (c) Range compression

Fig. 6. Ideal point target simulation result based on CCS

Pick 3 random point targets from the imaging result and carry out the quality evaluation. The result is shown in Table 2.

Table 2. Point target quality evaluation result based on CCS

Target	Azimuth	Range	PSLR/dB		ISLR/dB	
	Resolution/m	Resolution/m	Azimuth	Range	Azimuth	Range
1	0.888	3.33	-13.39	-34.337	-10.20	-24.375
2	0.897	3.34	-13.39	-34.337	-10.188	-24.375
3	0.890	3.33	-13.38	-34.337	-10.188	-24.375

Note. PSLR—peak side-lobe rate; ISLR—integral side-lobe rate.

Fig. 6 analyzes the CCS-based MIMO SAR imaging result and testifies the feasibility of CCS imaging. In order to compare with the traditional Chirp signal imaging result, Fig. 7 demonstrates the imaging result where, in the traditional single-transmitting single-receiving mode, the Chirp signal, under the same simulation condition, is used as the transmitting signal.

Fig. 7 (a) shows the point target imaging result based on Chirp signal, and Fig. 7 (b) and Fig. 7 (c) give the azimuth and range profile based on Chirp signal respectively.

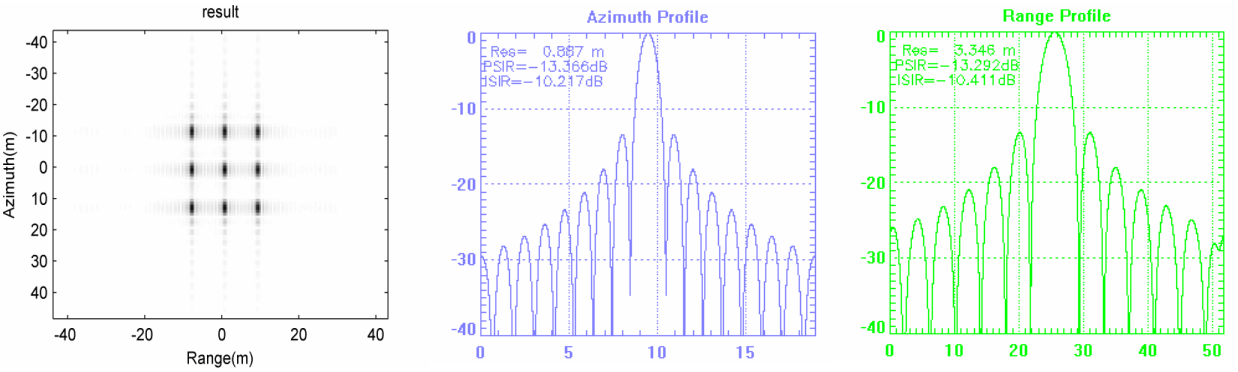

(a) Point target imaging result (b) Azimuth compression (c) Range compression

Fig. 7. Ideal point target simulation result based on Chirp signal

Similarly, pick 3 random point targets from the imaging result and carry out the quality evaluation. The result is shown in Table 3.

Table 3. Point target quality evaluation result based on Chirp signal

Target	Azimuth	Azimuth	PSLR/dB		ISLR/dB	
	Resolution/m	Resolution/m	Azimuth	Azimuth	Azimuth	Azimuth
1	0.888	3.33	-13.366	-13.292	-10.217	-10.411
2	0.897	3.34	-13.365	-13.292	-10.217	-10.411
3	0.890	3.33	-13.366	-13.292	-10.217	-10.411

Fig. 8 shows the Barker mode-based imaging result in the traditional single-transmitting single-receiving mode and the Barker mode takes the length of 13. Fig. 8 (a) represents the Barker mode-based point target imaging result, and Fig. 8 (b) and Fig. 8 (c) give the azimuth and range profile based on Barker mode.

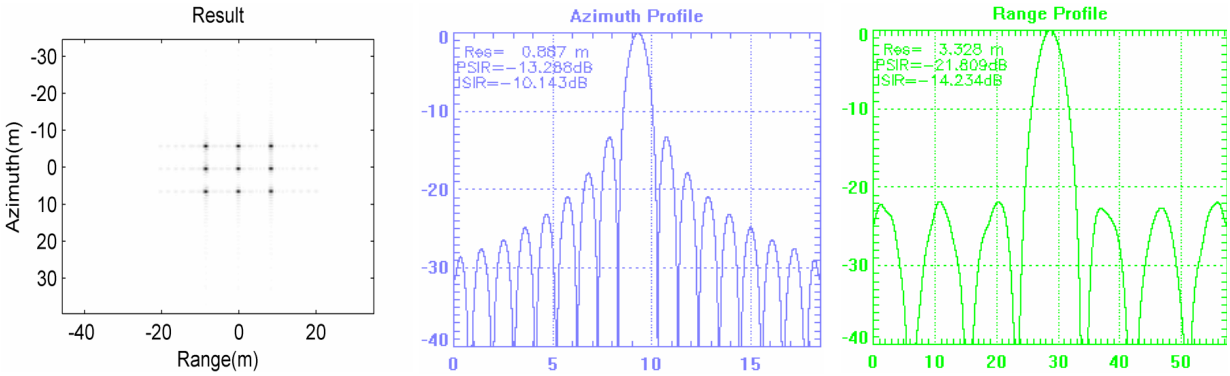

(a) Point target imaging result (b) Azimuth compression (c) Range compression

Fig. 8. Ideal point target simulation result based on Barker sequence

Similarly, pick 3 random point targets from the imaging result based on Barker sequence and carry out the quality evaluation. The result is shown in Table 4.

Table 4. Point target quality evaluation result based on Barker sequence

Target	Azimuth	Range	PSLR/dB		ISLR/dB	
	Resolution/m	Resolution/m	Azimuth	Range	Azimuth	Range
1	0.888	3.328	13.288	21.809	10.143	14.234
2	0.890	3.333	13.289	21.817	10.146	14.233
3	0.890	3.33	13.290	21.766	10.142	14.233

Combine the index analysis from Fig. 6 to Fig. 8 and from Table2 to Table 4. From the range dimension, the point target satisfies the ideal impulse response function; from the range and azimuth profile, the compression property of complementary sequence (-34.3dB) is better than the value of Chirp signal (-13.2dB) and Barker code (-21.8dB), without the main-lobe expansion and increasing the peak side-lobe rate and promising the range resolution simultaneously; different channels are free from co-channel interference and the anti-interference ability is improved due to the orthogonality of CCS. By applying CCS to the orthogonal MIMO SAR system, side-lobe output can be well suppressed, the peak side-lobe rate is improved on the basis of unchanged resolution and the anti-interference ability is enhanced.

Table 5 shows the comparison of PSLR and ISLR between this paper and other references [16-17]. From Table.5, the imaging result based on CCS is better than the other two. Therefore we can conclude that CCS-based MIMO radar system can greatly improve the target performance.

Table 5. Comparison between this paper and other documents

	Reference[16]	Reference[17]	This paper
PSLR/dB	-18.2	-25.6	-34.3
ISLR/dB	-5.7	-16.2	-24.4

4 Conclusion

According to the CCS side-lobe cancellation characteristic, this paper primarily discussed the MIMO SAR imaging problem based on CCS and phase compensation. The simulation result demonstrated that CCS-based MIMO SAR has better point target index comparing to Chirp signal and Barker code.

Acknowledgements

This work was partly supported by National Natural Science Foundation of China under grants 61401407 and partly supported by Engineering Planning Project in Communication University of China 2017XNG1712.

References

[1] J. Wu, Y. Bai, L.Y. Zhang, Distributed time synchronization in wireless sensor networks via second-order consensus algorithms, Transactions of Tianjin University 21(2)(2015) 113-121.

[2] H. Deng, Polyphase code design for orthogonal netted radar systems, IEEE Transaction on Signal Processing 52(11)(2004) 3126-3135.

[3] M. Yang, S. Zhang, B. Chen, A novel signal processing approach for the multi-carrier MIMO radar, Journal of Electronics & Information Technology 31(1)(2009) 147-151.

[4] B. Liu, C. Han, J. Miao, OFD-LFM signal design and performance analysis for MIMO radar, Journal of University of Electronic Science and Technology of China 38(1)(2009) 28-31.

[5] J.-H. Kim, M. Younis, A. Moreira, W. Wiesbeck, Spaceborne MIMO synthetic aperture radar for multimodal operation, IEEE Transactions on Geoscience and Remote Sensing 53(5)(2015) 2453-2466.

[6] W. Wang, MIMO SAR chirp modulation diversity waveform design, IEEE Geoscience and Remote Sensing Letters 11(9)(2014) 1644-1648.

[7] N. Duan, D. Wang, X. Ma, Approach of wave-number domain imaging for the MIMO radar system with small-squint angle, Journal of Air Force Radar Academy 22(3)(2008) 169-172.

[8] H. Wang, Y. Su, Y. Zhu, MIMO radar imaging based on spatial spectral-domain filling, ACTA ELECTRONICA SINICA 36(6)(2009) 1242-1246.

[9] S.F. Li, J. Chen, L.Q. Zhang, Application of complete complementary sequence in orthogonal MIMO SAR system, Progress in Electromagnetics Research C. 13(2010) 51-66.

[10] A. Currie, Wide-swath SAR imaging with multiple azimuth beams, in: Proc. IEE Colloquium on Synthetic Aperture Radar, 1989.

[11] M. Suess, B. Grafmueller, R.A. Zahn, A novel high resolution, wide swath SAR systems, IEEE International Geoscience and Remote Sensing Symposium (IGARSS) 3(2001) 1013-1015.

[12] P. Huang, Y. Deng, H. Qi, The echo processing method for multiple-transit and multiple-receive space-borne SAR, Journal of Electronics & Information Technology 32(5)(2010) 1056-1060.

[13] L. Wang, J. Xu, L. Nian, Moving target detection and imaging for spaceborne SAR in wide-swath based on repeated usage of space-time equivalent samplings, Signal Processing 25(12)(2009) 1871-1877.

[14] A. Currie, M. A. Brown, Wide-swath SAR, IEE Proceeding-f 139(2)(1992) 122-135.

[15] S.F. Li, J. Chen, L.Q. Zhang, Y.Q. Zhou, Construction of quadri-phase complete complementary pairs applied in MIMO radar systems, in: Proc. the 9th International Conference on Signal Processing (ICSP), 2008.

[16] L. Hu, H. Liu, S. Wu, Orthogonal waveform design for MIMO radar via constrained nonlinear programming, Systems Engineering and Electronics 33(1)(2011) 64-68.

[17] X. Du, T. Su, X. Wang, W. Zhu, B. Jin, L. Zhang, Golay complementary sequence with space time coding for MIMO radar waveform design, Journal of Electronics & Information Technology 36(8)(2014) 1966-1971.